
This paper was awarded in the IV International Competition (1995/96) "First Step to Nobel Prize in Physics" and published in the competition proceedings (*Acta Phys. Pol. A* **92** Supplement, S-21 (1997)). The paper is reproduced here due to kind agreement of the Editorial Board of "Acta Physica Polonica A".

SIMULATION OF CHARGED PARTICLE MOTION IN JUPITER'S MAGNETOSPHERE

M.S. MAHJOURI

Alholton High School, 6520 Freetown Road, Columbia, MD 21044, USA

Abstract

Particle motion in the Jovian magnetodisc is simulated in a rigidly corotating frame at radial distances from 50 to 150 Jovian radii. Results are compared with existing Pioneer and Voyager data to determine the accuracy of the simulation model. Particle orbits are classified into three distinct classes based on disjoint formations in phase space, and certain orbits are shown to have chaotic properties. The simulation is used to determine specific energies required to escape the magnetosphere through the neutral plane centered at the magnetic equator. The model should help to explain the detailed features observed for different charged particle species and energies within the Jovian magnetosphere, and will also provide a predictive and analytical tool for dealing with Galileo observations.

PACS numbers: 94.30.Hn, 52.20.Dq

1. Introduction

Energetic charged particles play an important role in Jupiter's magnetosphere. The Pioneer 10/11 and the Voyager 1/2 missions, during their separate encounters with Jupiter, made measurements that allow for a derivation of the magnetic field surrounding the planet. Analysis of the data has revealed that within the magnetosphere there exists an equatorially elongated magnetic field that is stronger than the general dipole (c.f. Figs. 1.0, 1.1). This elongation can be modeled by considering the presence of a thin disc of current flowing in the direction of the azimuth, or magnetodisc, that extends radially from the planet along the magnetic equatorial plane to at least 150 planetary radii (R_j).

It is well known that charged particles follow spiral orbits along dipole field lines, tending to bounce back and forth between the two planetary poles. In Jupiter's magnetic field, such particles may become temporarily trapped in the magnetodisc, bouncing back and forth within the magnetodisc until they escape to continue the gyrating in the dipolar region outside of the disc. At low magnetic latitudes (i.e. close to the magnetic equatorial plane), the magnetodisc causes great curvature in magnetic field lines. Few particles can negotiate these sharp magnetic turns and maintain the magnetic moment, which is proportional to the magnetic flux enclosed by the particle's spiral radius (gyroradius). Since the magnitude of magnetic force varies roughly as the inverse cube of radial distance from Jupiter, the gyroradii of energetic ions will increase accordingly. In some cases, the gyroradii of such ions may exceed the curvature radius of magnetic field lines within the magnetodisc and cause the ions to undergo nonadiabatic motion. This highly nonlinear motion, unpredictable within the magnetodisc, falls within the realm of deterministic chaos. Particles that travel through such orbits are discussed in Sec. 4. Once trapped inside the magnetodisc, a particle's motion can be broken down into two components:

a “bouncing” motion perpendicular to the magnetodisc, and a semicircular motion on the magnetodisc plane. The semicircular motion in the magnetodisc plane can cause the particle to drift radially outward, to the extent that it travels outside the effective realm of the magnetosphere. It is shown in Sec. 6 that the probability for such ions to escape is highly dependent on initial injection energy.

All physical predictions are based on a computer code that will model particle motion in Jupiter’s magnetosphere. This motion is determined by integrating the Lorentz force using the best existing model for the Jovian magnetosphere. At a given energy, the code simulates injection with an isotropic pitch angle distribution, and allows for isolation of different particles and different points of injection.

The available data reveal that the velocity distributions of ions are not isotropic in phase-space, a factor that is most likely due to the stretching effect of the magnetodisc on the magnetic field. The validity of the computer experiment described herein is verified by garnering distributions that agree with the observed data. Section 5 shows that the distributions obtained through this simulation are consistent with those detected by the Pioneer spacecraft.

The Galileo spacecraft, which will begin orbiting Jupiter in December 1995, carries several instruments that will measure characteristics of Jupiter’s magnetosphere, including its magnetic field, plasma, and energetic charged particle populations. The Energetic Particle Detector (EPD) will provide information regarding the activity of high energy ions and electrons within the Jovian magnetosphere. This simulation will be used as a tool to predict and explain observations made by the spacecraft.

Because Jupiter’s magnetic axis is at an angle to its rotation axis, the magnetodisc tends to flap up and down causing periodic fluctuations in data. Since this behavior is similar to that expected to exist in pulsars, a detailed study of Jupiter’s magnetodisc may also provide insight into issues of astrophysical interest.

2. Preliminaries

2.1. General definitions associated with charged particles in a magnetic field

The time rate of change of momentum for a particle with charge q and mass m in a magnetic field \mathbf{B} and electric field \mathbf{E} is described by the experimentally determined Lorentz force, which is (in the units of Gaussian CGS)

$$\frac{d\mathbf{p}}{dt} = q\mathbf{E}(\mathbf{x}, t) + \frac{q}{c}\mathbf{v}(t) \times \mathbf{B}(\mathbf{x}, t), \quad (1)$$

where \mathbf{x} is the particle’s position vector from a given reference point, \mathbf{v} is the particle’s velocity, and c is the speed of light (approximately 3×10^{10} cm/s). According to special relativity, the momentum \mathbf{p} is given by

$$\mathbf{p} = \gamma m\mathbf{v}, \quad (2)$$

where the Lorentz factor is

$$\gamma = \left(1 - \frac{v^2}{c^2}\right)^{-\frac{1}{2}}. \quad (3)$$

To clarify the nature of the force in Eq. (1), we derive an expression for the time rate of change of kinetic energy W by taking the dot product of the velocity with both sides of Eq. (1) to show that

$$\frac{dW}{dt} = q\mathbf{v} \cdot \mathbf{E}. \quad (4)$$

Equation (4) shows that, in the absence of an electric field (i.e. $\mathbf{E} = 0$), kinetic energy is constant. Put simply, a magnetic field cannot change the kinetic energy of a particle. Equation (1) can be solved analytically to show that particles in a static uniform magnetic field, i.e. $\mathbf{E} = 0$ and $\mathbf{B} = \text{constant}$, spiral (gyrate) along field lines. The previous description can be applied to a particle’s

instantaneous position in the magnetosphere when the magnetic field varies with position but can be assumed to be constant with time. Such particles have an instantaneous orbital frequency (gyrofrequency) of

$$\Omega \equiv \frac{qB}{\gamma mc} = \text{gyrofrequency} \quad (5)$$

and orbital radius (gyroradius)

$$r_g \equiv \frac{v_{\perp}}{\Omega} = \text{gyroradius}, \quad (6)$$

where v_{\perp} is the component of velocity that is perpendicular to the local magnetic field \mathbf{B} . Equation (5) allows us to define the period of one gyration as

$$\tau = \frac{2\pi}{\Omega} = \text{gyroperiod}. \quad (7)$$

We also define a pitch angle α , which is the angle between the velocity vector \mathbf{v} and the magnetic field \mathbf{B} at any point \mathbf{x} , such that

$$\alpha = \tan^{-1}(v_{\perp}/v_{\parallel}), \quad (8)$$

where v_{\parallel} is the component of the particle's velocity parallel to the direction of the local magnetic field.

2.2. Adiabatic invariants

Equations (1–8) allow us to draw an important conclusion regarding the predictability of particle motion in a known magnetic field. If the magnetic field varies slowly over space, i.e.

$$\frac{r_g |\nabla \mathbf{B}|}{B} \ll 1 \quad (9)$$

and slowly over time, i.e.

$$\frac{\tau |\partial \mathbf{B} / \partial t|}{B} \ll 1, \quad (10)$$

then the ratio of perpendicular component of kinetic energy, W_{\perp} , to the magnitude of the magnetic field, B , is approximately invariant. This is called the first adiabatic invariant, or magnetic moment, and is expressed as follows:

$$\mu = \frac{W_{\perp}}{B} = \frac{\frac{1}{2} m v_{\perp}^2}{B} = \frac{\frac{1}{2} m v^2 \sin^2 \alpha}{B}. \quad (11)$$

For Jupiter, conditions (9) and (10) are true at high magnetic latitudes where the magnetic field is well approximated by that of a magnetic dipole, and the first adiabatic invariant (11) is a constant of the motion.

Consider a system in which there is no electric field \mathbf{E} parallel to the time-independent magnetic field. Then a particle's kinetic energy remains constant, and can be expressed as

$$W = \frac{1}{2} m (v_{\perp}^2 + v_{\parallel}^2) = \frac{1}{2} m v_{\parallel}^2 + \mu B = \text{const}. \quad (12)$$

In a field where the first adiabatic invariant is conserved, Eq. (11) shows that, as the magnetic field strength increases (e.g. as a particle following a dipole field line gets closer to a pole), the pitch angle must also increase. At a given ‘‘mirror point’’ (where the pitch angle increases to 90 degrees) v_{\parallel} decreases, goes through zero and changes signs. For certain \mathbf{B} fields that satisfy (9) and (10), e.g., those of dipolar forms, a charged particle oscillates periodically between two such mirror points, and it is possible to define a second conserved quantity

$$J = \oint p_{\parallel} ds = 2\sqrt{2m} \int_{m_1}^{m_2} \sqrt{W - \mu B(s)} ds$$

$$= 2\sqrt{2m\mu} \int_{m_1}^{m_2} \sqrt{B_m - B(s)} ds, \quad (13)$$

where p_{\parallel} denotes momentum parallel to the magnetic field, s describes distance traveled along the field line, m_1 and m_2 are mirror points, and B_m is the magnitude of the magnetic field at either mirror point. Equation (13) defines the second adiabatic invariant of motion, and is constant in a field satisfying (9) and (10).

The motion of a particle gyrating in a field in which the first and second adiabatic invariants are conserved is easily predictable if the magnetic field strength is known. Such motion can be expected for charged particles in the dipolar region (well above or below the magnetodisc) of the Jovian field. However, as particles move into the current disc, the radial component of the magnetic field changes direction, and conditions (9) and (10) are not satisfied. In this region, particles undergo nonadiabatic motion; the highly nonlinear dynamics of nonadiabatic motion can produce observed anisotropies in the measured densities of high energy protons [1].

2.3. Guiding center theory

When conditions (9) and (10) are satisfied, a charged particle's motion consists of a velocity component along \mathbf{B} plus a slow drift velocity perpendicular to \mathbf{B} . Using (1) and averaging particle motion over a gyroperiod yields the following expression for momentum [2]:

$$m \frac{d^2 \mathbf{R}(t)}{dt^2} = q \mathbf{E}(\mathbf{R}(t), t) + \frac{q}{c} \frac{d\mathbf{R}(t)}{dt} \times \mathbf{B}(\mathbf{R}(t), t) - \mu \nabla B(\mathbf{R}(t)), \quad (14)$$

where $\mathbf{R}(t)$ represents the particle's guiding center at time t . Taking the cross product of \mathbf{B} with both sides of (14), assuming time independent \mathbf{B} and \mathbf{E} fields, and considering the case that the particle's parallel velocity is much greater than its perpendicular guiding center velocity, it is possible to express the component of the particle's guiding center velocity perpendicular to the magnetic field as follows:

$$\frac{d\mathbf{R}_{\perp}}{dt} = \frac{c \mathbf{E} \times \mathbf{B}}{B^2} + \frac{c \mu \mathbf{B} \times \nabla B}{q B^2} + \frac{c m v_{\parallel}^2 \mathbf{B} \times (\widehat{\mathbf{B}} \cdot \nabla) \widehat{\mathbf{B}}}{q B^2}. \quad (15)$$

The three terms on the right hand side of Eq. (15) represent the " $\mathbf{E} \times \mathbf{B}$ drift," "grad- \mathbf{B} drift," and "curvature drift", respectively. In all terms, both \mathbf{B} and \mathbf{E} are evaluated at the guiding center \mathbf{R} . In a planetary dipole with a cylindrical coordinate system centered on the planet, the effects of the drifts for higher energy particles in Eq. (15) would be most pronounced in the azimuthal (ϕ) component. As will be shown in Sec. 6, the effects of the guiding center drifts can couple with rapid oscillations induced by the current disc for higher energy particles, setting a particle's orbit on a hyperbolic drift trajectory and allowing it to effectively escape the magnetosphere from inside the magnetodisc.

2.4. Jupiter's magnetic field

Magnetometers carried by the Pioneer 10/11 and Voyager 1/2 spacecraft measured Jupiter's magnetic field. In addition, charged particle detectors on Pioneer 10 recorded ten hour flux rates of energetic charged particles. This periodic fluctuation of measurements is caused by the existence of a current sheet aligned with the magnetic pole and at an angle to the rotational pole. Randall [3] and Van Allen et al. [4] have used the fact that charged particles tend to follow magnetic field lines to deduce a 10 degree tilt angle between the planet's rotational and dipole axes. Northrop et al. [5] interpreted delays in expected particle fluxes as due to the finite Alfvén wave propagation, i.e., the delay between planetary rotation and subsequent rotation of the outer parts of the distant magnetosphere, such that field lines deviate from the meridian plane and have an azimuthal component. Smith et al. [6] interpret 10 hour particle fluxes as due to the existence of an extended current sheet along the magnetic equator. Goertz et al. [7] use the Pioneer 10 magnetometer and charged particle observations to produce a mathematical model for the Jovian magnetic field. The magnetic field consists of the superposition of a dipole

field with that produced by a current disc in the plane of the magnetic equator. In cylindrical coordinates, the two fields are given by

dipole:

$$B_\rho = \frac{3Mz\rho}{(\rho^2 + z^2)^{\frac{5}{2}}}, \quad (16a)$$

$$B_\phi = 0, \quad (16b)$$

$$B_z = \frac{M(2z^2 - \rho^2)}{(\rho^2 + z^2)^{\frac{5}{2}}}, \quad (16c)$$

current sheet:

$$b_\rho = \frac{b_0 D}{\rho r^\alpha} \tanh(z/D) - \frac{ab_0 z}{\rho r^{\alpha+2}} \{\ln[\cosh(z/D)] + C\}, \quad (17a)$$

$$b_\phi = -6.12 \times 10^{-3} e^{\rho/500} \rho b_\rho(\rho, z), \quad (17b)$$

$$b_z = \frac{ab_0}{r^{\alpha+2}} \{\ln[\cosh(z/D)] + C\}, \quad (17c)$$

where α, b_0, C, D are constants determined by fitting the Pioneer 10 data (Table (1.0)), α is the exponent of magnetodisc radial variation, b_0 is the disc field variable, C is the dimensionless constant, D is the disc thickness. In Eqs. (16), the constant M is the Jovian dipole moment, found in Table (1.1).

Table 1.0. Magnetic field constants fit to Pioneer 10 magnetometer data.

α	b_0	C	D
0.7	9×10^{-2} G	10	$1R_J$

Table 1.1. Pertinent physical values for Jupiter.

Planetary radius	Dipole moment	Planetary rotation period	Orbital frequency
$1R_J = 7.1492 \times 10^9$ cm	4.2 Gauss $\times R_J^3$	10 h	$\omega = 1.745 \times 10^{-4}$ rad/s

Although the Voyager data is more recent, Voyager models of the magnetic field are reliable only out to 30 Jovian radii, and the goal is to simulate particle motion in the range of 50–150 Jovian radii. Therefore, the field provided by Goertz et al. [7] with Pioneer 10 data is used. The magnetic field model can then be expressed as

$$\mathbf{B}(\rho, \phi, z) = \hat{\mathbf{e}}_\rho(B_\rho + b_\rho) + \hat{\mathbf{e}}_\phi(B_\phi + b_\phi) + \hat{\mathbf{e}}_z(B_z + b_z). \quad (18)$$

Figures 1.0–1.5 display the field strength and components as labeled, and clearly illustrate the local minimum, or magnetic “well” in the field magnitude created by the current disc near the magnetic equatorial plane. Figure 1.6 shows that the radius of curvature for any field line is minimum on the magnetic equatorial plane, and that this curvature radius decreases as radial distance from the planet increases. The “sharp turns” of field lines about the magnetic equator, i.e., inside the current disc, cause the direction of the magnetic field to change abruptly. This rapid spatial variation of the magnetic field inside the magnetodisc does not satisfy Eq. (9), which requires a slow variation over space. Therefore, nonadiabatic and highly nonlinear motion near the current disc is to be expected.

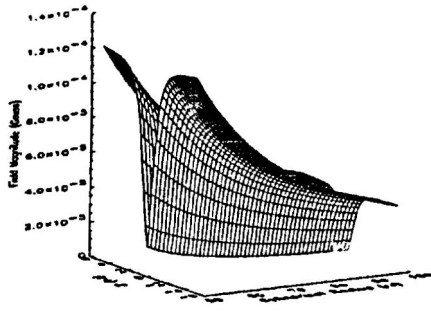


Fig. 1.0. Field strength.

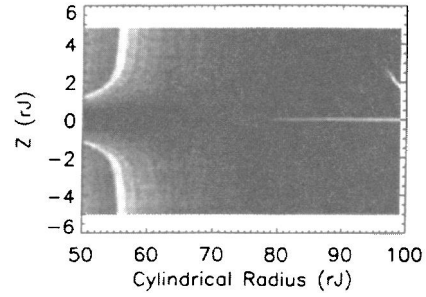


Fig. 1.1. Field strength.

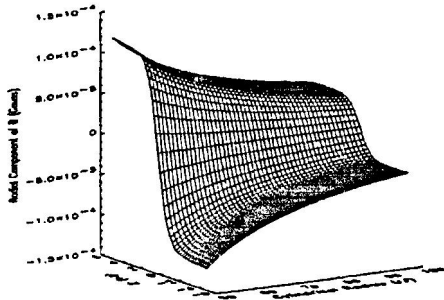


Fig. 1.2. Radial field.

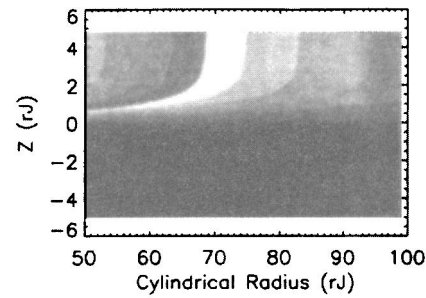


Fig. 1.3. Radial field.

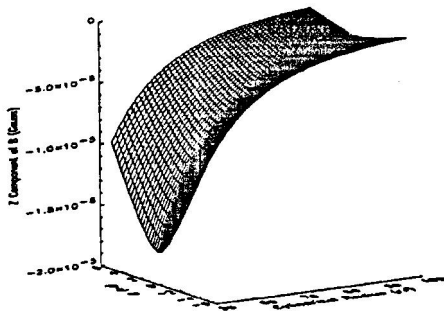


Fig. 1.4. Z field.

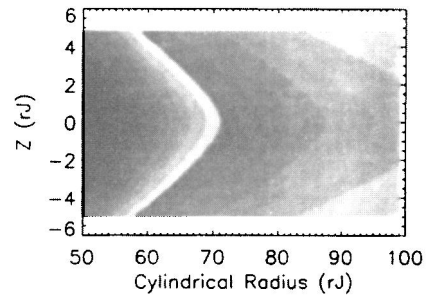


Fig. 1.5. Z field.

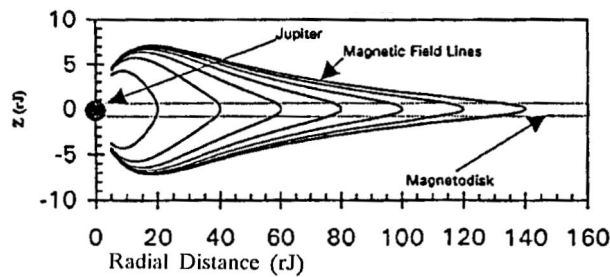


Fig. 1.6. Jovian field lines.

3. Basic method

Using the magnetic field model provided by Goertz et al. [7], we simulate charged particle motion through Jupiter's magnetosphere and into the magnetodisk. Particles are injected isotropically in velocity space. We perform different runs of the program by injecting electrons and various ion species, and systematically varying the particle energy to analyze motion within the magnetodisk.

To simplify calculations, we choose a reference frame that is corotating rigidly with the magnetospheric plasma that is trapped on magnetic field lines. In this corotating frame the

electric field due to rotating plasma vanishes. We account for the coriolis and centrifugal forces that arise in this noninertial reference frame, and transform (1), using the subscript r to denote that a function is evaluated in the rotating (noninertial) frame

$$\frac{dp_r}{dt} = \frac{q}{c} \mathbf{v}_r(t) \times \mathbf{B}(\mathbf{x}_r, t) + m\omega^2 \mathbf{r} + 2m\mathbf{v}_r \times \boldsymbol{\omega}, \quad (19)$$

$$\mathbf{r} = \hat{\mathbf{e}}_\rho \rho, \quad (20)$$

$$\boldsymbol{\omega} = \hat{\mathbf{e}}_z \omega, \quad (21)$$

\mathbf{B} is given by (18), \mathbf{v}_r denotes the particle's velocity in the corotating frame, ω is the angular velocity of the corotation frame about the rotation axis, and ρ is the particle's cylindrical radius as measured from the planet. To corotate with Jupiter's magnetosphere, we set ω equal to the rotational frequency of the planet, as given in Table (1.1). The centrifugal and coriolis forces, present in any rotating reference frame, are represented by the second and third terms of (19), respectively. Taking the scalar product of the rotational velocity with both sides of (19) yields a quantity that must be conserved during particle motion. This conserved quantity is the sum of the particle's kinetic energy and its centrifugal potential energy

$$\frac{1}{2}mv_r^2 + \frac{1}{2}m\omega^2\rho^2 = \varepsilon. \quad (22)$$

For calculating particle densities (i.e. simulating several thousand particle orbits), Eqs. (16) and (17) can be costly in terms of computer time. Calculations are simplified by evaluating the magnetic field on a two dimensional grid, and using a combination of table lookup and bilinear interpolation found in Ref. [8].

Integration of (19) for the three components of position and corresponding velocity is accomplished using a fifth-order Runge–Kutta numerical integration procedure. An adaptive stepping algorithm found in Ref. [9] and coded in *Numerical Recipes in C (Vers 2.0)* is slightly modified and used to speed the integration process. A random number generator, also found in *Numerical Recipes in C (Vers. 2.0)* is used to generate random initial conditions. Numerical accuracy is monitored by assuring that the orbital invariant (22) remains constant to within 1 part in 10^3 .

4. Single orbits

Particle orbits in the Jovian field can be classified roughly into three categories: bounded, transient, and stochastic. Figures 2.0–2.1 show a transient orbit that characteristically follows the expected dipolar orbit until it hits the current disc. Once inside, it bounces around unpredictably, but quickly exits the magnetodisc to continue gyrating in a predictable fashion. The time spent within the magnetodisc is very small, and once “outside” the particle continues gyrating in the dipolar region of the field until it “mirrors” back into the magnetodisc. Another type of orbit, not shown, is the bounded or “regular” orbit, that can only exist for particles injected in the magnetodisc. Bound orbits are permanently trapped within the magnetodisc. Figures 2.2–2.5 show stochastic orbits. Such orbits exhibit adiabatic characteristics outside the magnetodisc region, but become trapped for long periods of time within the current disc. Once within the current disc, the particle undergoes motion similar to that of a bounded orbit, but with far less periodicity. Unlike bounded orbits, however, stochastic orbits eventually exit the magnetodisc region. Figures 2.6–2.7 show particle motion in a dipole field, and serve as an example of pure adiabatic motion.

Stochastic orbits temporarily trapped within the magnetodisc cross the magnetic equatorial plane many times, while transient orbits tend to cross it once or twice. The number of equatorial crossings of bounded orbits is unlimited. Particles are injected at a single point in the “neutral plane”, i.e., $z = 0$, and various components of motion at subsequent neutral plane crossings are recorded. This technique, titled the “Poincare surface of section”, allows otherwise undetectable

properties of the three different particle orbits to be explored. Figures 3.0–3.7 show particle behavior in a Poincare surface of section for various injection energies. Normalized particle velocities are recorded at plane crossings to show that the bound, transient, and stochastic orbits populate finite boundaries within phase space. The regions created by bounded orbits consist of the tightly bounded concentric circular formations, each of which represents the crossings of a single trapped particle, and whose radius depends upon injection velocity. It becomes clearly visible that the bound orbits are confined to a particular “circle”, which implies that their motion is governed by some invariant [10]. Stochastic orbits populate the region outside the concentric circles, which is characterized by the large distribution of crossing points. No unperturbed orbit can cross between the stochastic and bounded regions. Stochastic orbits present a remarkable characteristic, namely, that the distance in phase space between two orbits with nearly identical injection coordinates will diverge exponentially with time. Stochastic orbits from particles injected at any differential initially stochastic region in the phase space will entirely cover the stochastic region, regardless of what region is chosen. The space is shown to be “sticky”, as stochastic orbits can come arbitrarily close to the bounded region and become trapped for indefinitely long time periods, a property shown in Fig. 6, where no bounded orbits exist (particles are injected outside of the magnetodisc), but the outline of the bounded region is marked by “sticky” stochastic orbits. This characteristic is most clearly evident in Fig. 2.5, where the circular bounces of the stochastic orbit in the ρ – ϕ plane mimic bounded orbit motion. Transient orbits populate the sparse regions characterized by the seeming “bald spots” on the figures. Transient orbits cross the neutral plane only a few times per magnetodisc entry, so their presence in a space populated by “full-time” bounded orbits and “part-time” stochastic orbits is relatively scarce. Accordingly, Fig. 3 shows only a few points in the transient region. Transient orbits can, however, move into the stochastic region from a few particular transient points after occupying a series of transient regions.

If plotted in three dimensional phase space, the crossing velocities shown in Fig. 3 would map directly onto a sphere. Figures 3.3–3.7 demonstrate that such a sphere would be bilaterally symmetrical upon the radial velocity axis. Such an assertion is rather obvious, since a bounded orbit would require oppositely changing z velocity at every crossing in order to maintain its circular orbit on the surface of section. The near symmetry about the horizontal line bisecting Figs. 3.3–3.7 serves to validate the accuracy of the simulation model.

The structure of the phase space formation is highly dependent on the z component of the magnetic field. A particle under the influence of two perfectly antiparallel field lines would undergo either a figure eight motion around both field lines, or it would spiral around one field line. To analyze chaotic motion, a quantity

$$\kappa \equiv \sqrt{\frac{\psi_c}{r_g}} \quad (23)$$

is defined, and the field line equatorial radius of curvature, ψ_c , is calculated to be

$$\frac{|-M/\rho^3 + ab_0C/\rho^{\alpha+2}|}{\{(3M/\rho^4 + b_0/D^2\rho^{\alpha+1} - ab_0C/\rho^{\alpha+3})^2 + [he^{\rho/500}\rho b_0(b_0/D^2\rho^{\alpha+1} - aC/\rho^{\alpha+3})^2]\}^{\frac{1}{2}}}. \quad (24)$$

As κ approaches unity, the level of chaos in the magnetodisc, measured by the percentage of stochastic orbits, is maximized. For a one dimensional system depending only on z , Buchner and Zeleny [11] have shown this behavior analytically and Chen and Palmadesso [10] have proven it numerically. Karimabadi et al. [12] arrive at this result for a family of two dimensional field models similar to the Jovian field model in (16–18). The values of κ , gyroradius, and curvature radius based on the field (16–18) are represented in Fig. 4. Buchner and Zeleny [11] found that for $\kappa \ll 1$, there is still a significant amount of chaos within the system. Particle behavior near the current sheet is then not only nonadiabatic, but also chaotic.

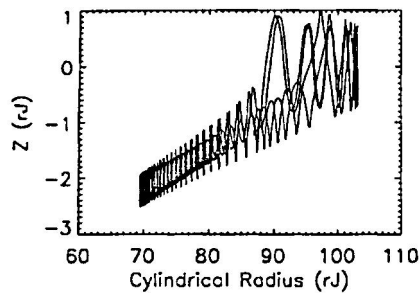


Fig. 2.0

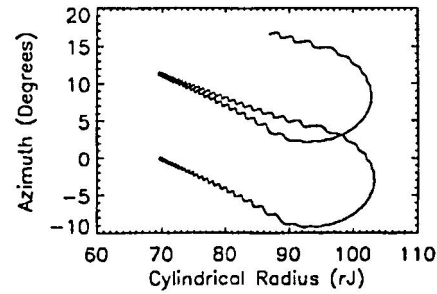


Fig. 2.1

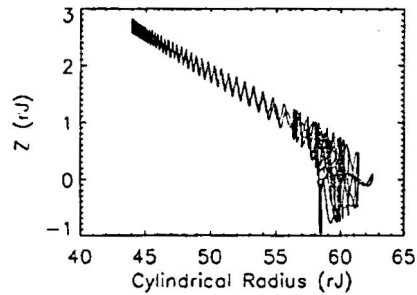


Fig. 2.2

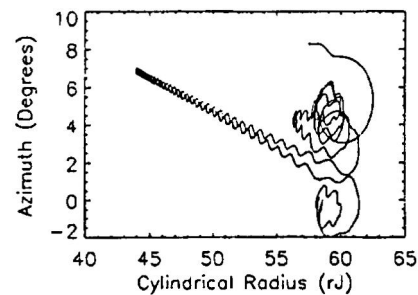


Fig. 2.3

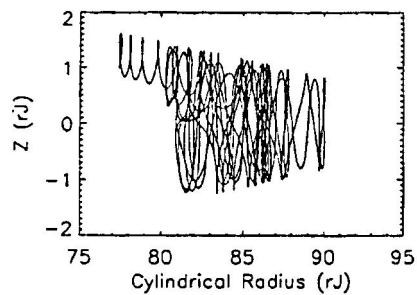


Fig. 2.4

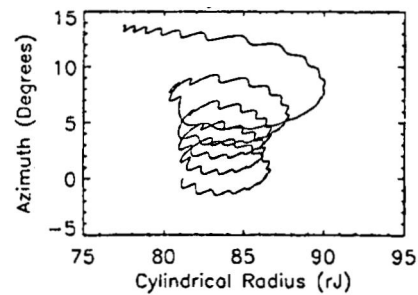


Fig. 2.5

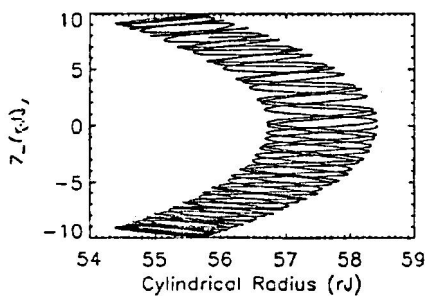


Fig. 2.6

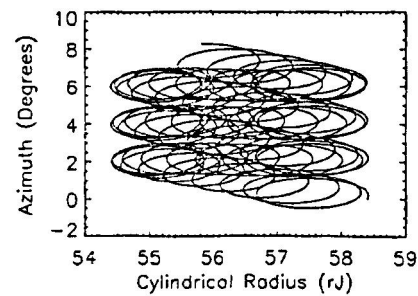


Fig. 2.7

Upon first glance, Fig. 3.3 fails to show the structure evident for particles of lower energies. The 10 meV particles yield a κ value that is approximately 17% smaller than that for the 10 keV particles. Accordingly, the bounded space is replaced by stochastic orbits, which indicates a greater amount of chaos, as (23) predicts. This effect is evident in the diminution of bound orbit islands as injection energy increases. However, a 17% decrease in κ cannot virtually eliminate all bounded orbits, as is suggested by Fig. 3.3. Each bounded particle seems confined to a semicircle in the $v\rho-v\phi$ plane. It is entirely possible that the bounded orbits do exist in their complete circular form, but that they escape the system radially before they can complete their circular phase space formation. This is more plausible than the complete elimination of bounded orbits, and leads to the concept of energy drop-off that is discussed in Sec. 6. In fact, the ratio

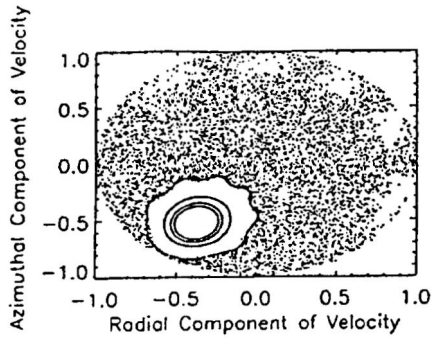


Fig. 3.0. 10 KeV protons.

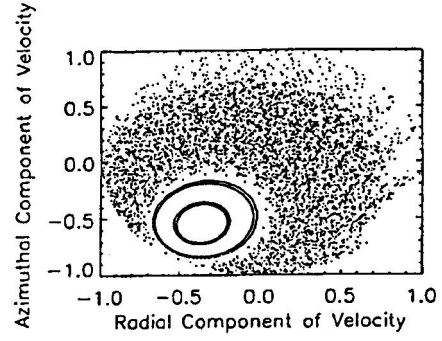


Fig. 3.1. 100 KeV protons.

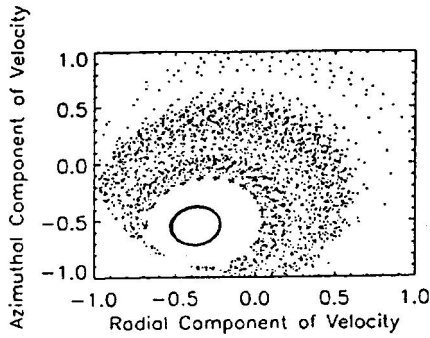


Fig. 3.2. 1 MeV protons.

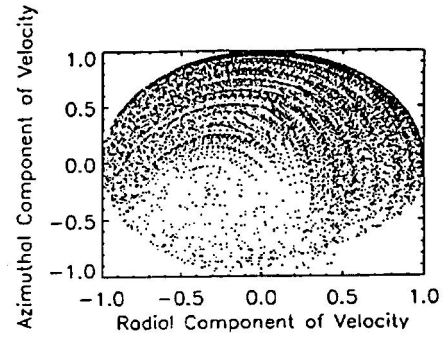


Fig. 3.3. 10 MeV protons.

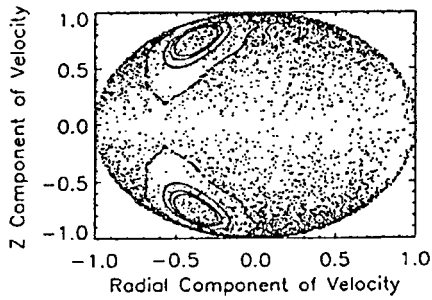


Fig. 3.4. 10 KeV protons.

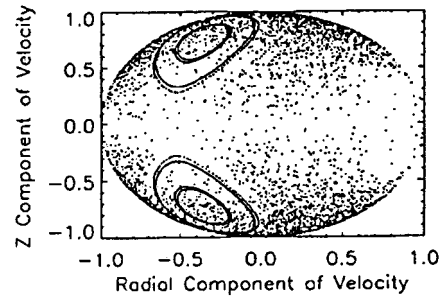


Fig. 3.5. 100 KeV protons.

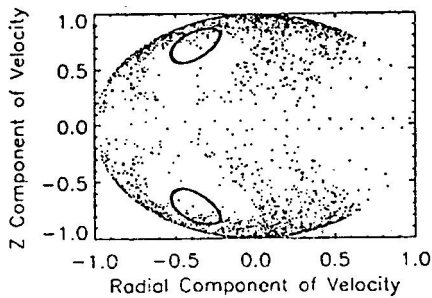


Fig. 3.6. 1 MeV protons.

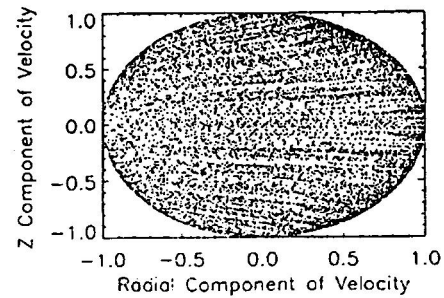


Fig. 3.7. 10 MeV protons.

of particles that escaped radially to particles that remained trapped indefinitely in Fig. 3.3 was much greater at 10 meV than at the lower energies. A slightly greater number of points lie in the positive radial velocity hemisphere (Fig. 3.7 shows this best) and a large majority also lie on the positive azimuthal hemisphere (Fig. 3.3).

Thus, there is a tendency for 10 meV protons to head in the positive ρ - ϕ direction, the direction of escape. The radial component of velocity does appear to be cycling in the relatively

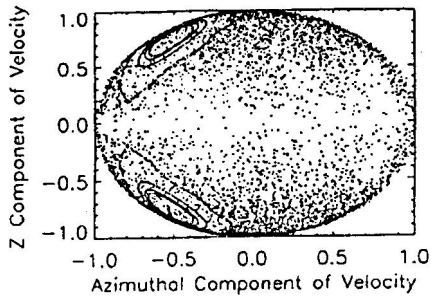


Fig. 3.8. 10 KeV protons.

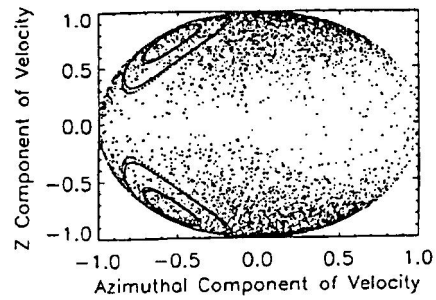


Fig. 3.9. 100 KeV protons.

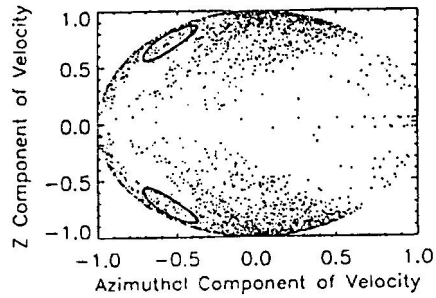


Fig. 3.10. 1 MeV protons.

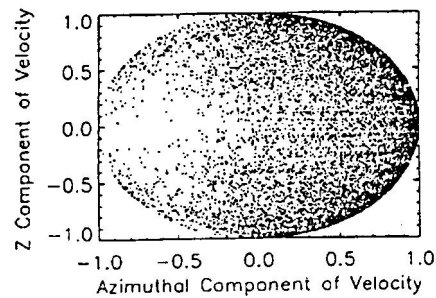


Fig. 3.11. 10 MeV protons.

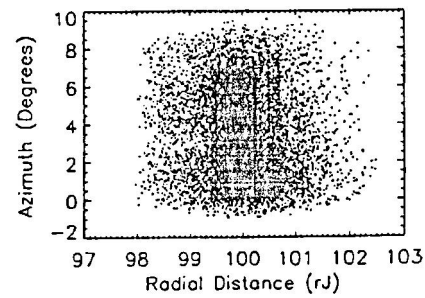


Fig. 3.12. 10 KeV protons.

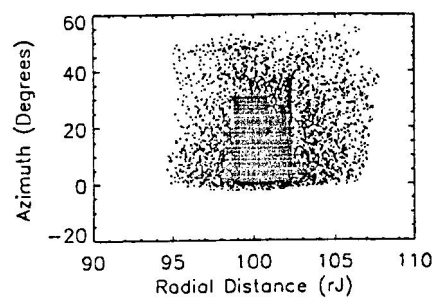


Fig. 3.13. 100 KeV protons.

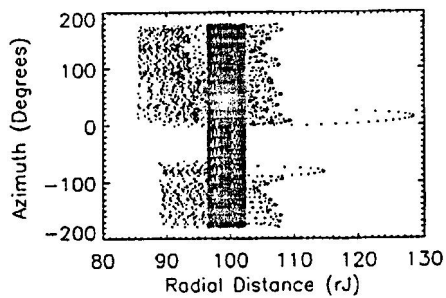


Fig. 3.14. 1 MeV protons.

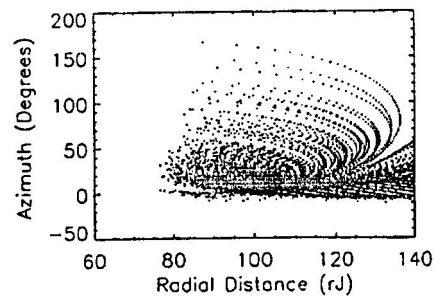


Fig. 3.15. 10 MeV protons.

expected way, but, assuming there are no “double loops”, the particle must always travel in the positive azimuthal direction to satisfy the surface of section. The 10 meV particles follow a serpentine motion, and their crossings with the neutral plane trace out a semicircle.

5. Probable regions

Figure 5 shows distributions of spatial density within $10 R_J$ for protons injected uniformly in the radial range from 50 to $150 R_J$, with z -component of $\pm 2.5 R_J$. The pitch angle distribution is isotropic at injection. The distributions are relatively symmetric about the z -axis as expected. The curved “root-like” appearance of the densities in Fig. 5 is consistent with the field model in

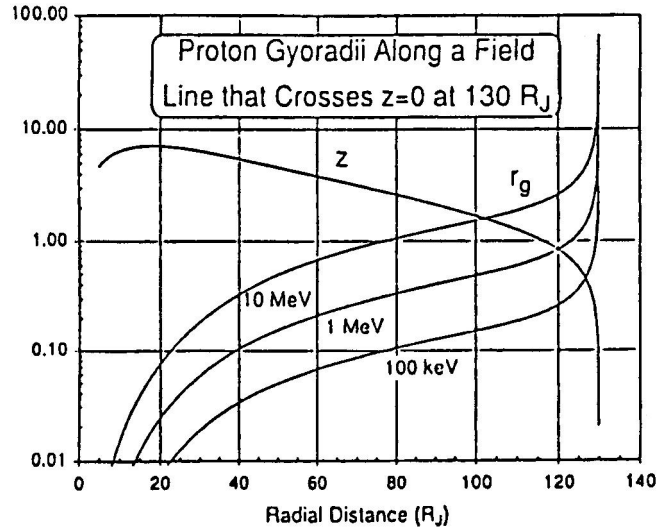


Fig. 4.0

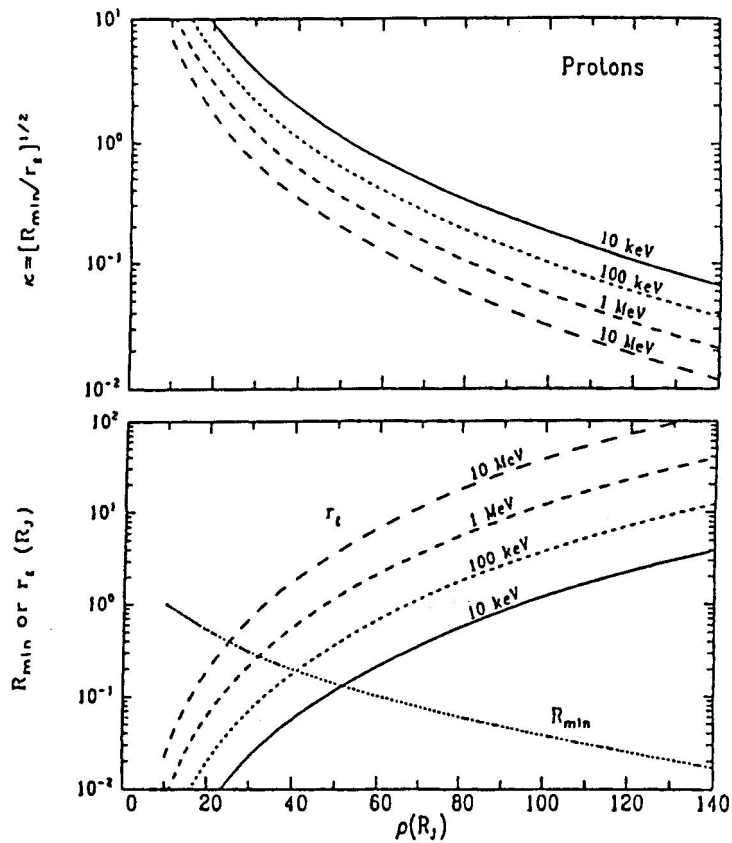


Fig. 4.1

Fig. 1, and can be attributed to the cutoff of the radial component of initial injection. The density enhancement evident within $z = \pm 0.5R_J$ shows that the particles are being temporarily trapped within the magnetodisc, again, as expected. With the current disc oscillating as the planet rotates, these trapped particles in the magnetodisc account for the square-wave modulation of particle count rates detected by the University of Iowa instrument aboard Pioneer 10 in the region of $50\text{--}100R_J$, as shown in Fig. 1 in Ref. [7]. The simulation is consistent with these data.

A highly informative feature in the spatial surface of section plots (azimuth versus radius), most obvious for 10 meV particles, is the subtle appearance of “tracks” extending radially outward, away from the clumped region. As Figs. 3.15 (10 meV protons) and 6.5–6.6 (10 meV

protons) indicate, there is a current disc “escape route” for higher energy particles. Because of their escape, these make negligible contribution to the density, especially when compared to stochastic orbits that mimic bounded particles. However, the escaping particles are dense enough to leave a small track behind.

6. Effect of initial energy and injection ρ

6.1. Analytic argument

The field given by

$$\mathbf{B}(\rho) = \frac{\hat{\mathbf{e}}_z b}{\rho^\alpha} \quad (25)$$

is inversely proportional to some power of the cylindrical distance from the planet. The ρ , ϕ , z components of the Newton–Lorentz equations for such a field are as follows:

$$\ddot{\rho} - \rho \dot{\phi}^2 = \frac{qb}{mc} \dot{\rho} \rho^{1-\alpha}, \quad (26a)$$

$$\rho \ddot{\phi} + 2\dot{\rho} \dot{\phi} = -\frac{qb}{mc} \dot{\rho} \rho^{-\alpha}, \quad (26b)$$

$$\ddot{z} = 0. \quad (26c)$$

Multiplying (26b) by ρ and transforming it into differential form shows that for $\alpha \neq 2$ the quantity

$$\rho^2 \dot{\phi} + \frac{qb}{mc} \frac{\rho^{2-\alpha}}{2-\alpha} = \rho_0^2 \dot{\phi}_0 + \frac{qb}{mc} \frac{\rho_0^{2-\alpha}}{2-\alpha} \quad (27)$$

is conserved. Defining the local gyrofrequency at injection ρ as

$$\Omega_0 = \frac{q(b/\rho_0^\alpha)}{mc} = \frac{qB_0}{mc} \quad (28)$$

such that (27) becomes a quadratic of the form

$$\left(\frac{\rho}{\rho_0}\right)^2 \dot{\phi} + \frac{\Omega_0}{2-\alpha} \left(\frac{\rho}{\rho_0}\right)^{2-\alpha} = \frac{\Omega_0}{2-\alpha}. \quad (29)$$

The next step is to find the maximum cylindrical radius given initial ρ and initial velocity. To simplify matters, it is assumed that the injection velocity has only a ρ component ($v = v_\rho$), i.e., it is perpendicular to the magnetic field. Then, it is possible to substitute the velocity at any point divided by the initial gyrofrequency for the initial gyroradius. Then, (29) transforms into

$$\xi^{\alpha-1} - \frac{\rho_0/r_{g0}}{2-\alpha} \xi^{\alpha-2} + \frac{\rho_0/r_{g0}}{2-\alpha}, \quad (30)$$

where

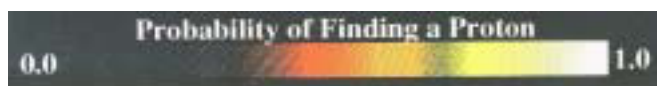
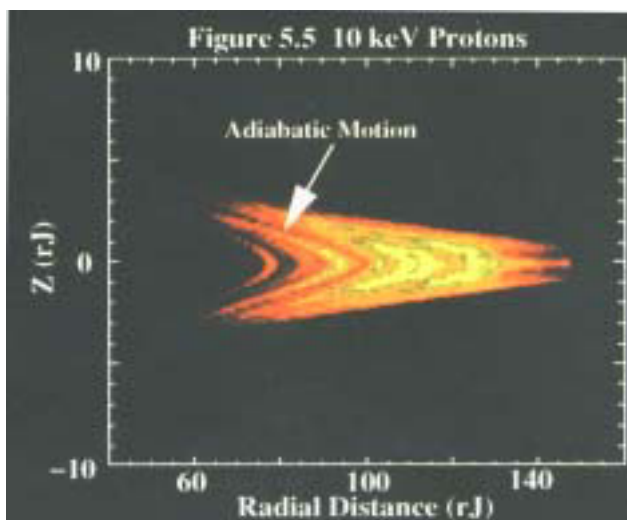
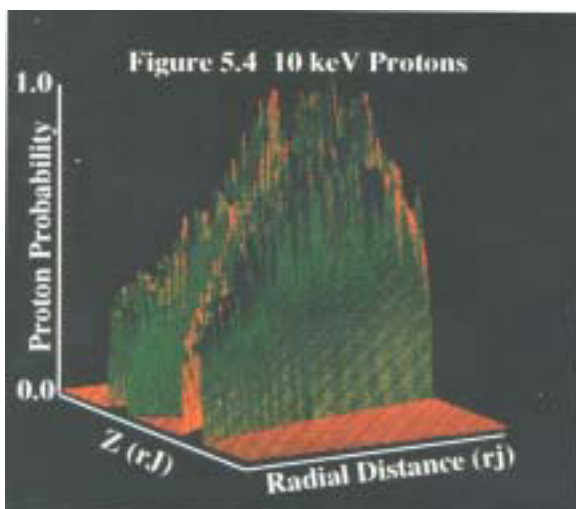
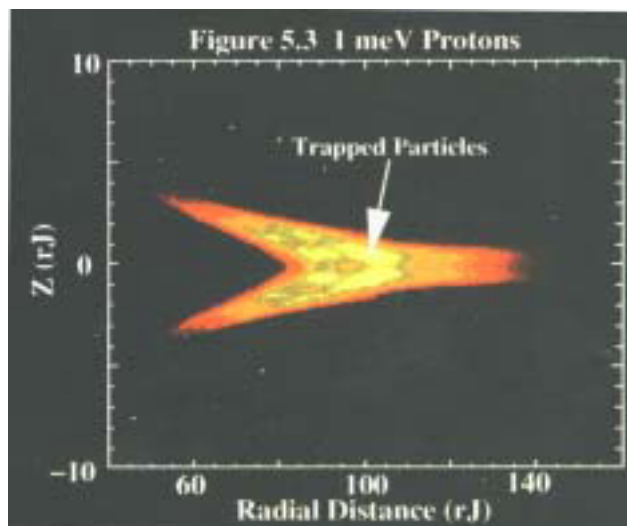
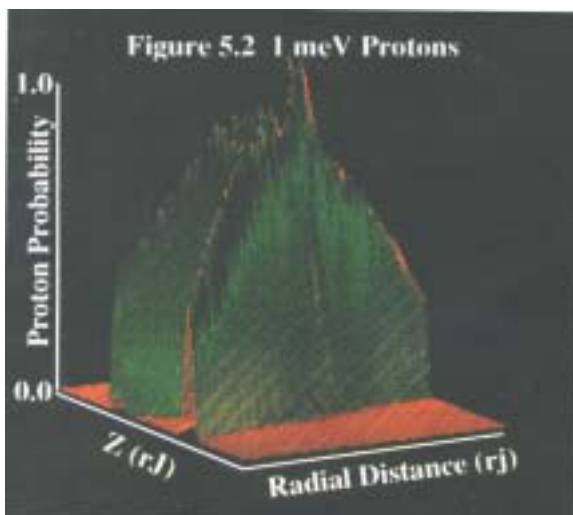
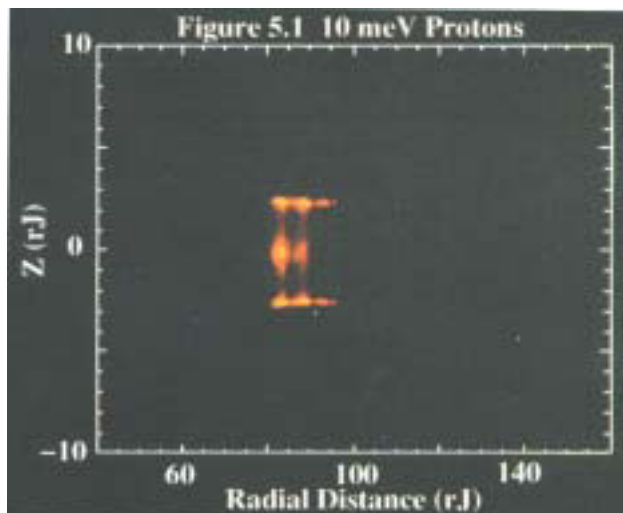
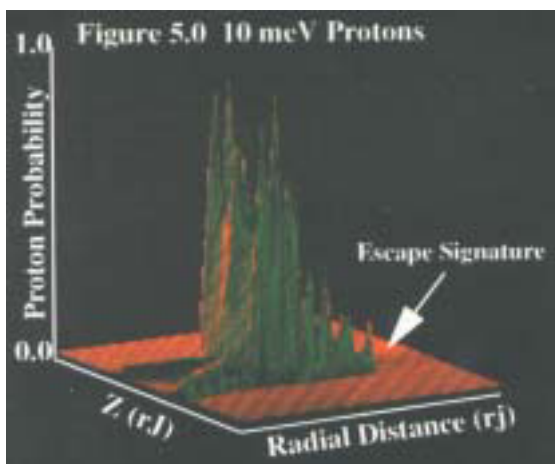
$$\xi \equiv \frac{\rho_{\max}}{\rho_0}. \quad (31)$$

For a particle to escape, the initial conditions must be such (30) has an imaginary root, i.e., ρ goes to infinity. According to Pioneer 10 data, the exponent of the Jovian magnetic field comes out to about 2.7. It is appropriate to estimate (30) for $\alpha = 3$ (the fall off rate for a magnetic dipole), in which case (30) has the physically significant root

$$\xi = \frac{\rho_0}{2r_{g0}} \left\{ 1 - [1 - 4(r_{g0}/\rho_0)]^{1/2} \right\}, \quad (32)$$

which reveals that, for the specified simplifications, a particle can theoretically escape through the $z = 0$ plane if its initial energy satisfies

$$W_0 > \frac{m\Omega_0^2 \rho_0^2}{32}. \quad (33)$$



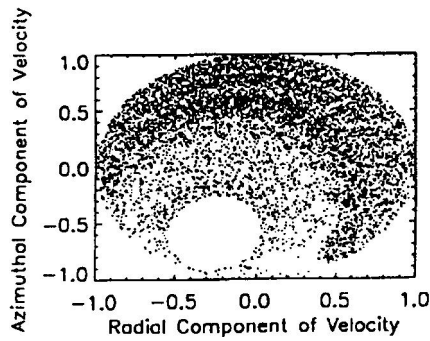


Fig. 6.0. 52 rj.

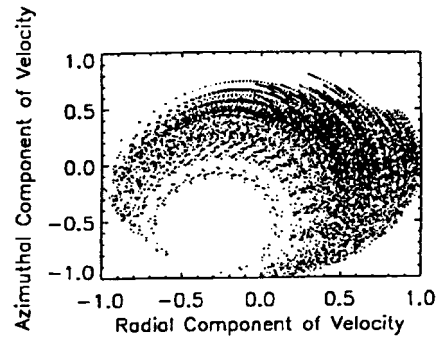


Fig. 6.1. 68 rj..

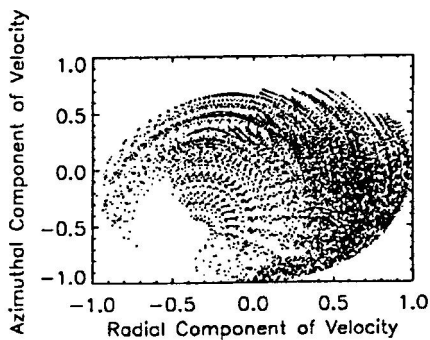


Fig. 6.2. 82 rj.

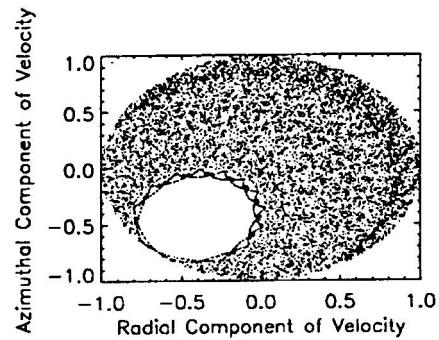


Fig. 6.3. Positron at 82 rj.

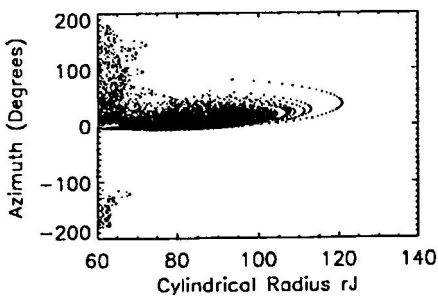


Fig. 6.4. 52 rj.

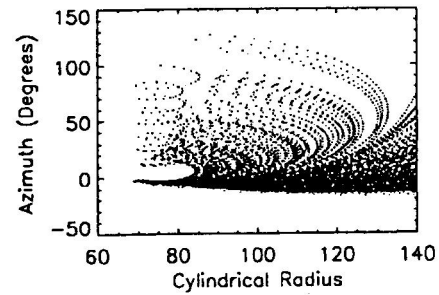


Fig. 6.5. 68 rj.

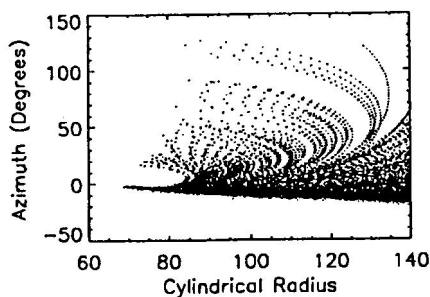


Fig. 6.6. 82 rj.

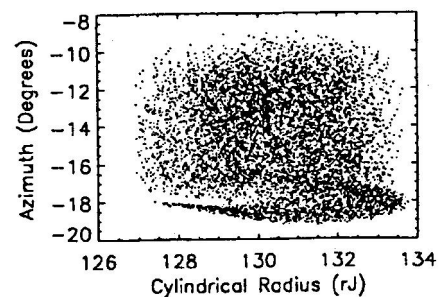


Fig. 6.7. Positron at 82 rj.

6.2. Radial dependence

The probability of escaping through the magnetodisc is also dependent on injection radius. It is prudent to use surface of section plots to illustrate this dependence. In Fig. 6, 10 meV protons are injected at $z = \pm 2.5R_J$, to simulate injection into the current disc from high latitudes. This eliminates bound orbits, which can only exist if the particle is injected in the current disc, reemphasizes stochastic orbit properties, and simulates a more realistic situation. The positron is plotted (Figs. 6.3, 6.7) because its small mass relative to that of a proton will allow it to map

along the field line out to the radius where the field line crosses the equatorial plane. It serves as an accuracy “check” of the simulation.

Figures 6.0–6.3 show the evolution of the phase-space coordinates as radial distance increases. The preponderance of points tending toward the positive (outward) radial velocity hemisphere indicate a clear tendency toward escape as injection radial distance increases. The position plots (Figs. 6.4–6.6) show the particles performing a giant semicircular motion through subsequent crossings. As injection radius increases, however, fewer and fewer particles reach the “reversal-point” required to complete the loop and head back inward. As they circle outward, the fields is also getting weaker, and the curvature radius of their semicircle is increasing. A fraction of these orbits can become radially unbounded, and not come back inward, even if a radial “cutoff” boundary is not specified.

6.3. Numerically calculated energy drop-offs

The preceding findings suggest the presence of an escape mechanism in the magnetodisc, by which particles can radially exit the magnetosphere. To prove this numerically, we set up a simulation in which we inject particles at a single radius, but still at $z = \pm 2.5R_J$. The four energies of interest are: 10 meV, 1 meV, 100 keV, and 10 keV. This covers the energy range relevant to energetic particle detectors on the Pioneer, Voyager, and Galileo spacecraft. The effect of injection radius, demonstrated qualitatively for 10 meV particles in Fig. 6, is tested quantitatively by limiting injection to a single radius and varying that radius in subsequent runs. For each injection radius, four separate simulations are executed, one for each of the aforementioned energies. The number of particles that travel beyond a ρ boundary of $200R_J$ in a constant time are considered to “escape” the magnetodisc. Figure 7 shows the fundamental result of this research. The probability of escape via the magnetodisc is clearly dependent on

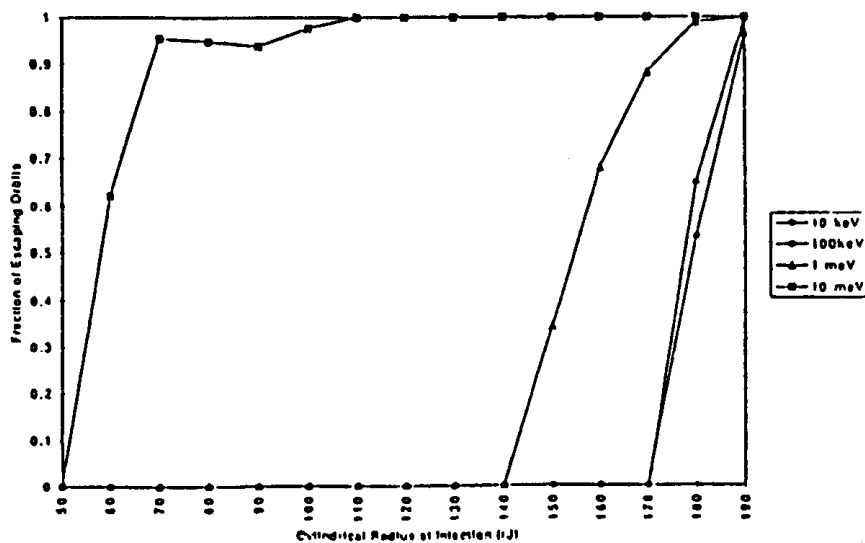


Fig. 7. Escape probability vs. radial distance of injection ($Z = 2.5R_J$).

injection energy and ρ . Once a given particle species is injected from a certain escape radius as determined by Fig. 7, all particles of that energy proceed to escape to the predefined boundary. The probability of escape increases with injection energy and injection ρ . The error in the calculations required to establish Fig. 7 is confined to $\pm 5\%$.

7. Discussion

We have assumed that particles propagate along the time-independent, smooth magnetic field in Eqs. (16) and (17). However, naturally occurring magnetic fields, like those in Jupiter’s magnetosphere, fluctuate on a range of times and scales. These magnetic fluctuations can scatter charged particles. The pitch angle of a particle can be perturbed by Coulomb collisions, plasma

waves, or small-scale field irregularities. Such effects could cause the particle to “jump” to an otherwise restricted region of phase space and cross boundaries in the Poincare surface of section. A more accurate simulation model would incorporate pitch angle scattering to account for such effects as mentioned above. However, Cheng and Decker [1] demonstrated the “relative unimportance of scattering, even when the scattering substantial populates the regular (bounded) orbit region of phase space”.

The particles in this simulation are treated as test particles, i.e., their presence does not affect the existing field. As has been shown, these particles do tend to drift in the direction of the current, so drift motion will actually augment the current density. Since the contribution of these particles to the current disc is small, it is reasonable to ignore the self consistent aspects of the problem.

We have not specified the origin of the injected protons in our simulation. One possible source is the Jovian ionosphere. The Voyagers discovered active volcanoes on the moon Io, probably set off by the tidal pumping between Europa and Ganymede, and Jupiter. The volcanic material is ejected at approximately 1.05 kilometers/sec, enough to escape the moon. Io appears to be the principle contributor of matter in the Jovian magnetosphere, secondary of course to Jupiter. Another contributor of particles may well be from outside the system, as Goertz et al. [7] predicted the existence of open field lines.

This research was carried out only for protons. It is well known that Jupiter’s magnetotail contains high abundances of heavier ions such as oxygen and sulfur, that evidently originate at Io. The radial escape mechanism will also apply to these heavier ions. We are currently investigating this radial loss process for these heavier ions for comparison with spacecraft measurements. Also, Jupiter’s magnetosphere is able to trap highly relativistic electrons. Our trial simulation of positrons, displayed in Fig. 6.7, shows clearly that electrons will also undergo nonadiabatic motion in Jupiter’s deep magnetotail. We are also actively investigating the motion of such relativistic electrons in the Jovian magnetodisc. The results of this research can also be compared with spacecraft observations of relativistic electrons.

Acknowledgments

The author is extremely grateful to R.B. Decker for his time, patience, notes, thoughts, discussion, use of office, use of facilities, and anything else I forgot. I would also like to thank my parents, teachers, and JHUAPL. This work was supported by no grants and I received no other assistance.

References

1. A.F. Cheng, R.B. Decker, *J. Geophys. Res.* **97**, 1937 (1992)
2. T.G. Northrop, *The Adiabatic Motion of Charged Particles*, Wiley, New York (NY) 1963
3. B.A. Randall, in: *The Magnetospheres of Earth and Jupiter*, Ed. V. Formisano, D. Riedel, Dordrecht 1975, p. 353
4. J.A. Van Allen, D.N. Baker, B.A. Randall, D.D. Sentman, *J. Geophys. Res.* **79**, 3559 (1974)
5. T.G. Northrop, C.K. Goertz, M.F. Thomsen, *J. Geophys. Res.* **79**, 3579 (1974)
6. E.J. Smith, L. Davis, Jr., D.E. Jones, P.J. Coleman, Jr., D.S. Colburn, P. Dyal, C.P. Sonett, A.M.A. Frandsen, *J. Geophys. Res.* **79**, 3501 (1974)
7. C.K. Goertz, D.E. Jones, B.A. Randall, E.J. Smith, M.F. Thomsen, *J. Geophys. Res.* **81**, (1976)
8. W.H. Press, S.A. Teukolsky, W.T. Vetterling, B.P. Flannery, *Numerical Recipes in C*, sec. ed., Press Syndicate of the University of Cambridge, New York (NY) 1992
9. W.H. Press, S.A. Teukolsky, *Comput. Phys.* **6**, 188 (1992)
10. J. Chen, Palmadesso, *J. Geophys. Res.* **91**, 1499 (1986)
11. J. Buchner, L.M. Zeleny, *J. Geophys. Res.* **94**, 11, 821 (1989)
12. H. Karimabadi, P.L. Pritchett, F.V. Coroniti, *J. Geophys. Res.* **95**, 17, 153 (1990)